Environmental Science and Pollution Research (2023) 30:122482–122496
https://doi.org/10.1007/s11356-023-30836-7

RESEARCH ARTICLE

Rheological and mechanical performance analysis and proportion optimization of cemented gangue backfill materials based on response surface methodology

Xiaoxuan Wang[1] · Yuxia Guo[1,2,3] · Guorui Feng[1,2,3] · Xiaoli Ye[1] · Weiyang Hu[1] · Jiahui Ma[1]

Received: 17 May 2023 / Accepted: 30 October 2023 / Published online: 16 November 2023

Abstract

Cemented backfill mining is a green mining method that enhances the coal mining rate and the safety of mined-out regions. To transport the cemented gangue backfill material (CGBM) into the mined-out regions, it is essential to ensure high flowability and adequate compressive strength after hardening. Based on the response surface methodology (RSM), 29 experiments were conducted in this paper to test the yield stress and plastic viscosity of CGBM slurry. Cubic specimens with dimensions of 100 mm were prepared and underwent uniaxial compression tests to obtain the compressive strength at a curing age of 28 days. Quadratic polynomial regression models were established for yield stress, plastic viscosity, and compressive strength to explore the effects of fly ash content, water-cement ratio, mass concentration, and superplasticizer dosage on the properties of CGBM. Multi-objective optimization was conducted to determine the optimal material proportion of CGBM. The research results indicate that (1) the mass concentration most profoundly affected the yield stress and plastic viscosity of CGBM, and it increased with an increase in mass concentration. Fly ash content had an inverse relationship with compressive strength. Superplasticizer was found to improve the flowability and strength of CGBM. (2) The established response surface model could reflect the relationship between CGBM's material proportion and rheological and mechanical properties, and predict relevant parameters. (3) Multi-objective optimization determined the optimal proportion of CGBM to be 80% fly ash content, 54% water-cement ratio, 79% mass concentration, and 3% superplasticizer dosage. The research findings offer valuable guidance to mining backfill engineering.

Keywords Cemented gangue backfill material (CGBM) · Response surface method · Rheological properties · Mechanical properties · Multi-objective optimization

Introduction

Due to continuous coal extraction, issues related to difficult mining and destruction of the ecological environment have become increasingly prominent. In the quest for sustainable mining, it is crucial to balance environmental and resource-related concerns, thus promoting the widespread adoption of mine backfilling (Qian et al. 2007; Asr et al. 2019; Chugh and Behum 2014, Yilmaz et al. 2014). This technology utilizes abandoned coal gangue as its primary material which is then combined with cement, fly ash, water, and additives to create CGBM slurry that has a high filling efficiency and does not separate or settle. The slurry is transported through pipeline to the working face. This technology offers the advantage of not only controlling settlement and enhancing mining rates but also recycling solid waste deposited on the ground to create useful underground space (Feng et al. 2022; Sun et al. 2019; Zheng et al. 2006). Moreover, this technology is effective in mitigating safety issues such as goaf collapse and gas explosions and can bolster the overall security and dependability of mining processes (Deng et al. 2017; Feng et al. 2019; Ma et al. 2011).

Responsible Editor: Philippe Garrigues

✉ Yuxia Guo
gyx771221@163.com

[1] College of Mining Engineering, Taiyuan University of Technology, Taiyuan 030024, Shanxi, China

[2] Shanxi Province Coal-Based Resources Green and High-Efficiency Development Engineering Center, Taiyuan, Shanxi, China

[3] Shanxi-Zheda Institute of Advanced Materials and Chemical Engineering, Taiyuan, Shanxi, China

During the backfill mining process, the critical requirements are to ensure that the CGBM slurry has good pumpability during pipeline transportation and that it has sufficient strength after reaching the working face to support the deformation of the overlying strata. (Fei 1997; Xu et al. 2016; Wang et al. 2021). Reng et al. (2014) studied the effect of different fly ash contents on the rheological properties of filling slurry, the compressive strength, and dry shrinkage of filling bodies at different ages. Qi et al. (2022) replaced cement and fly ash in CGBM with biomass power plant ash and found that the flowability and uniformity of the freshly CGBM slurry can be significantly improved when 10% of cement or 20% of fly ash is replaced with biomass power plant ash. Wu et al. (2016) studied the mechanical properties and ultrasonic characteristics of CGBM with different fly ash contents under different mass concentrations and found that the compressive strength of the filling bodies was exponentially related to the corresponding ultrasonic pulse velocity at different mass concentrations. Wang et al. (2014) used waste stones and desert aggregate to prepare pastes and studied the rheological properties of pastes with different concentrations, finding that the mass concentration was the factor that most influenced the rheological properties and that the yield stress of the paste with waste stone as the coarse aggregate was greater. Yang et al. (2021) used computational fluid dynamics simulations to study the rheological properties of different slurries and established a pipeline resistance model, finding that mass concentration had the most significant impact on pipeline resistance. Peng et al. (2019) studied the influence of different types and dosages of binding materials on the rheological properties and bleeding rate of slurry, and preliminarily explored the pumping mechanism. Yin et al. (2012) carried out rheological experiments for filling slurry with different polycarboxylate superplasticizers, and derived a mathematical expression for calculating the slurry pipeline resistance under the condition of adding the superplasticizers. These studies provide strong support for the sustainable development of backfill mining. The rheological and mechanical properties of CGBM are influenced by factors such as mass concentration, the content of cementitious materials, and the use of water-reducing agents. However, there has been limited research conducted on the influence extent of their effects and the interaction between them.

Due to the numerous performance parameters and influential factors of filling materials, optimizing their properties usually requires a considerable number of experiments. This makes optimization work difficult. The response surface methodology is a method that combines mathematical and statistical methods. This methodology has the advantage of requiring fewer trials, delivering high precision, and achieving excellent predictive performance when studying the interaction effects among multiple factors (Allaix and Carbone 2011; Faravelli 1989; Li et al. 2019a, b). Hua et al. (2022) used RSM to study the effect of various coal-based solid wastes on the compressive strength of filling bodies, and found that the significance order of the factors on strength was fly ash > coal gangue > desulfurization gypsum > 1 : 1 mixture of gasification slag and bottom slag. Zhu et al. (2021) used the single-factor method to determine the appropriate range of mass concentration, fly ash content and fine gangue ratio in the filling slurry, and then used RSM to establish quadratic polynomial regression equations for the three factors and yield stress and plastic viscosity. Feng et al. (2015) replaced the fine and coarse aggregates in the filling slurry with waste concrete and studied the mechanism of their effects on the flowability and compressive strength of the filling slurry, and established corresponding regression models to obtain a reasonable filling material ratio. Thus, it can be inferred that response surface methodology can be employed for studying the impact of various factors on the performance of CGBM.

The purpose of this study was to analyze changes in fly ash addition, water-binder ratio, mass concentration, and superplasticizer dosage in the rheological and mechanical properties of CGBM, and to then develop a response surface model based on this analysis. Finally, the developed model was employed to optimize the material ratio. The research results could provide a basis for the proportion design of backfill mining.

Experimental methods

Raw materials

The binding materials utilized in this experiment were conventional Portland cement (P.O42.5, Taiyuan Shitou Co., Ltd) and fly ash (Fenxi Mining Group Power Plant). Coal gangue (Xinyang Coal Mine of Fenxi Mining Group) was employed as aggregate and sorted into three sizes: fine gangue (particle sizes < 5 mm), medium gangue (5–10 mm), and coarse gangue (10–15 mm). The experiment utilized 30% fine aggregates and 35% medium and coarse aggregates in the total mass of aggregates. The water reducer used in this experiment was poly-carboxylate superplasticizer (powder form, Shandong Hongxiang Building Admixture Co., Ltd). The mixing water was ordinary tap water. Figure 1 shows the SEM images of the raw materials. Table 1 and Fig. 2 present the key chemical compositions of the raw materials, obtained through the X-ray diffractometer analysis. Particle size distribution was measured using a laser particle size analyzer, and is presented in Fig. 3.

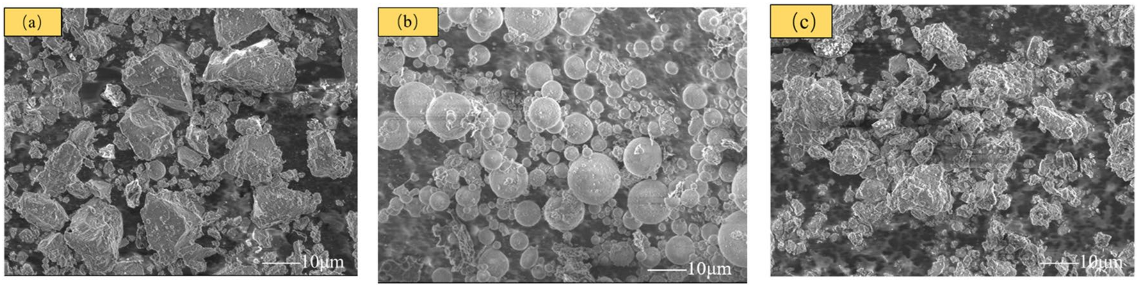

Fig. 1 SEM (**a**) Cement, (**b**) Fly ash, (**c**) Coal gangue

Table 1 Main chemical compositions of raw material

Materials	CaO	SiO_2	MgO	Fe_2O_3	Al_2O_3	TiO_2	Others
Cement%	65.08	22.36	1.27	3.46	5.53	-	2.30
Fly ash%	0.99	52.42	1.01	3.62	32.48	-	9.48
Coal gangue%	7.15	35.46	3.50	3.86	16.11	0.80	33.12

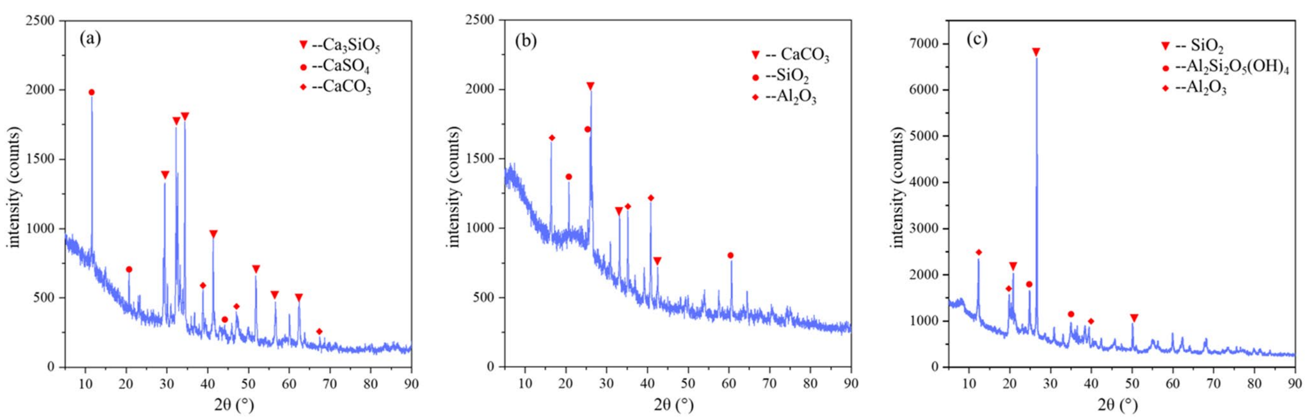

Fig. 2 XRD (**a**) Cement, (**b**) Fly ash, (**c**) Coal gangue

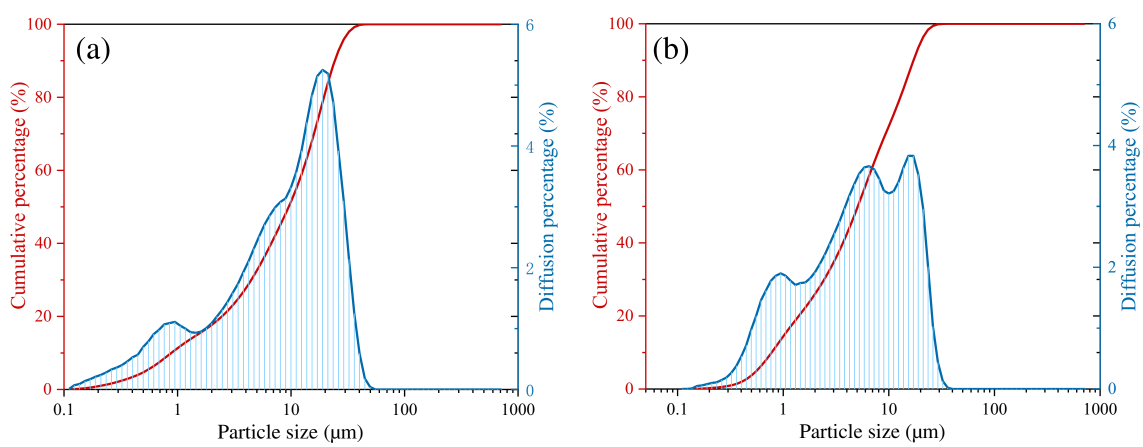

Fig. 3 Particle size distribution (**a**) Cement, (**b**) Fly ash

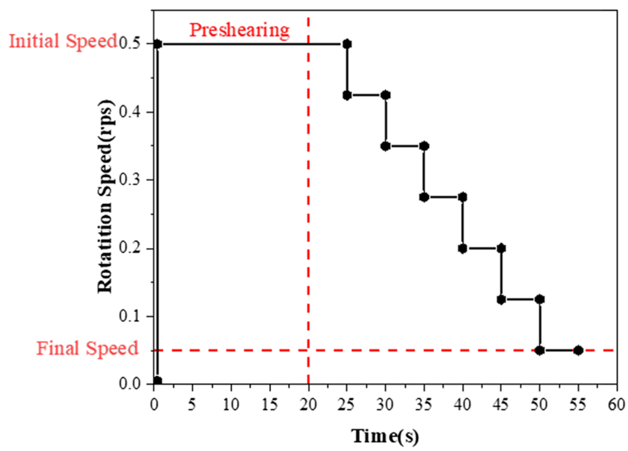

Fig. 4 Experimental flow chart

Testing methods

Rheological property testing

To get a fresh slurry, cement, fly ash, and coal gangue were mixed for 5 min in a mixer firstly, and then water and polycarboxylate superplasticizer were added and mixed for another 5 min. In order to evaluate its rheological properties, a Denmark Geremann Icar Rheometer was used for testing, and the experimental process and rheometer components are shown in Fig. 4. The rheometer employs a 127 mm high paddle blade with a 63.5 mm radius, and the barrel radius is 143 mm. During testing, the freshly mixed slurry was poured into the rheometer barrel, ensuring slurry covering the whole blade and reaching the scale line at the barrel edge. The test program initiated with a maximum speed of 0.5 r/s for 20 s and gradually reduces to a minimum speed of 0.05 r/s in equal increments (Ye et al. 2023). While testing, the rheometer collected seven torque-speed data points, with 5 s separating each test point. The schematic diagram of rheological test procedure is shown in Fig. 5. To calculate rheological parameters of yield stress and plastic viscosity, the Reynolds-Rheiner formula (Feys et al. 2013; Jiang et al. 2020) is employed, as follows:

$$\mathrm{T} = \frac{4\pi h \ln\frac{R_0}{R}}{\frac{1}{R^2}-\frac{1}{R_0^2}}\tau_0 + \frac{8\pi^2 h}{\frac{1}{R^2}-\frac{1}{R_0^2}}\mu N + \frac{8\pi^3 h(R_0+R)}{(\frac{1}{R^2}-\frac{1}{R_0^2})(R_0-R)}cN^2 \quad (1)$$

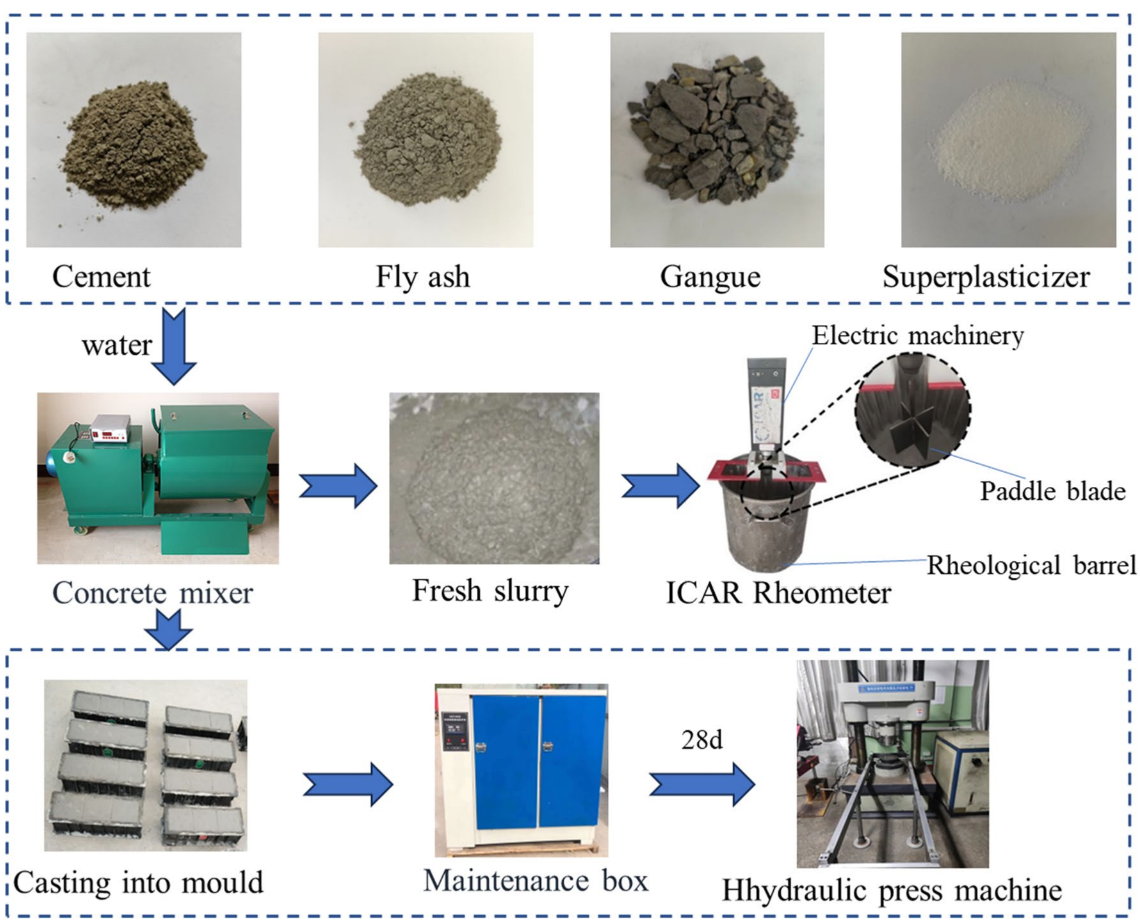

Fig. 5 Schematic diagram of rheological test procedure

$$\tau_0 = \frac{\frac{1}{R^2} - \frac{1}{R_0^2}}{4\pi h \ln\frac{R_0}{R}} G \tag{2}$$

$$\eta = \frac{\frac{1}{R^2} - \frac{1}{R_0^2}}{8\pi^2 h} H \tag{3}$$

$$c = \frac{\frac{1}{R^2} - \frac{1}{R_0^2}}{8\pi^3 h} \frac{\left(R_0 - R\right)}{\left(R_0 + R\right)} C \tag{4}$$

where τ_0 is the yield stress (Pa); η is the plastic viscosity (Pa·s); T is the torque (Nm); h is the blade height (mm); R is the blade radius (mm); and R_0 is the barrel radius (mm). c and C are constants; G is the coefficients of flow resistance; H is the coefficient of viscosity.

Mechanical property testing

The fresh slurry was poured into a three-part mold with dimensions of 100 mm × 100 mm × 300 mm. A vibrator was utilized to eliminate bubbles and ensure uniform filling. Afterwards, the surface was smoothened and covered with plastic wrap to prevent moisture evaporation and sealed around the edges. After standing for 24 h, the molds were removed, and the specimens were transferred into a curing box with a temperature of (20 ± 2) ℃ and relative humidity of not less than 95% for 28 days. A TAJW-2000 hydraulic servo Universal testing machine was used for the testing. The loading test began by slowly applying a load of 0.1 kN using the stress loading mode and then switching to the displacement mode to load the specimens at 0.8 mm/min (GB/T 50081-2002, 2002).

Experimental design based on RSM

The experiment was designed and analyzed by RSM with Box-Behnken Design (BBD), using Design-Expert software version 8.0.6.1. A quadratic model was applied to fit the response surface model and conducted significance tests on the model as well as outlier detection. Three levels of fly ash content (66–80%), water-binder ratio (50–60%), mass concentration (79–81%), and superplasticizer dosage (1–3%) were considered independent variables (Dong et al. 2013; Feng et al. 2022; Guo 2013), and yield stress, plastic viscosity, and compressive strength were considered response values in the analysis. To describe the structural ranges, three-level combinations were encoded as ± 1, 0 for the factorial point and the center point, respectively. To facilitate the analysis, the encoded values were presented in Table 2.

The correlation between the independent variables and the response values can be expressed using a second-order polynomial:

$$y(x) = a_0 + \sum_{i=1}^{n} a_i x_i + \sum_{i=1}^{n-1}\sum_{j=1}^{n} a_{ij} x_i x_j + \sum_{i=1}^{n} a_{ii} x_i^2 \tag{5}$$

where $y(x)$ is the objective function value; x_i is an independent variable, $i = 1, 2, \ldots\ldots, k$; a_o, a_i, a_{ij}, a_{ii} are undetermined coefficients.

The total number of runs was 29, including 5 center points, and the corresponding response values for each run were obtained through experiments, as shown in Table 3.

To evaluate the proposed polynomial model, the analysis of variance (ANOVA) was performed based on the determination coefficients R^2 and $R^2{}_{\text{adj}}$, as shown in Eqs. (4) and (5). To validate the accuracy of the model, a statistical significance test was conducted, as indicated by Eq. (6).

$$R^2 = 1 - \frac{SS_{residual}}{SS_{model} + SS_{residual}} \tag{6}$$

$$R_{adj}{}^2 = 1 - \frac{SS_{residual}/df_{residual}}{(SS_{model} + SS_{residual})/(df_{model} + df_{residual})} \tag{7}$$

$$Adequateprecision = \frac{max(n) - min(n)}{\sqrt{\sigma^2 Y}} \tag{8}$$

where df represents the degree of freedom; SS represents the sum of squares; n represents the number of experiments; σ^2 represents the residual mean square.

Table 2 The factors and levels of the response values

Independent variable	Symbol	Low level − 1	Medium level 0	High level 1
Fly ash content (%)	A	66	73	80
Water-binder ratio (%)	B	50	55	60
Mass concentration (%)	C	79	80	81
Superplasticizer dosage (%)	D	1	2	3

Table 3 The response surface experimental design and results

Run	Independent variables				Response values		
	Factor 1	Factor 2	Factor 3	Factor 4	Response 1	Response 2	Response 3
	A:fly ash content(%)	B:water-binder ratio(%)	C:mass concentration (%)	D:superplasticizer dosage (%)	Yield stress(Pa)	Plastic viscosity(Pa·s)	Compressive strength(MPa)
1	73	55	80	2	228.42	8.8	11.6
2	66	55	80	2	253.80	10.0	14
3	73	50	79	2	207.27	9.2	15.1
4	73	60	80	1	198.81	7.2	9.6
5	73	55	81	3	219.96	8.9	14.1
6	73	55	79	3	135.36	6.2	11
7	73	50	80	1	236.88	13.0	10.7
8	73	60	81	2	269.29	8.8	14.7
9	80	55	80	3	169.20	9.7	10.2
10	73	50	80	3	177.66	7.9	13.4
11	73	55	80	2	219.96	9.1	11.3
12	73	50	81	2	334.17	10.5	13.8
13	80	50	80	2	211.50	11.1	12
14	73	55	79	1	194.58	8.4	8.8
15	73	55	80	2	215.73	8.6	11.5
16	66	55	80	3	148.05	6.0	12.2
17	73	55	80	2	228.42	8.9	11.5
18	80	55	79	2	190.35	7.5	9.9
19	73	60	79	2	181.89	5.3	8.28
20	80	55	81	2	262.26	13.0	10.2
21	73	60	80	3	126.90	7.8	10
22	80	55	80	1	207.27	11.7	7.5
23	66	55	80	1	241.11	10.9	12.3
24	73	55	80	2	219.96	9.2	10.9
25	66	55	81	2	308.79	8.0	16.9
26	66	55	79	2	156.51	7.3	12
27	80	60	80	2	198.81	8.6	8.6
28	73	55	81	1	308.79	12.0	11.3
29	66	60	80	2	156.51	6.9	13.2

Table 4 The response surface functions and regression coefficients

Response values	Second order polynomial models	R^2	R^2_{adj}	C.V. %	Adequate precision
Yield stress	$222.21 - 2.11A - 24.32B + 52.43C - 33.40D + 21.15AB - 20.09AC + 13.75AD - 9.88BC - 2.85BD - 9.46CB - 10.69A^2 - 4.87B^2 + 23.45C^2 - 27.12D^2$	0.9850	0.9700	4.10	31.353
Plastic viscosity	$8.90 + 1.04A - 1.41B + 1.44C - 1.41D + 0.15AB + 1.21AC + 0.73AD + 0.55BC + 1.37BD - 0.24CD + 0.38A^2 - 0.15B^2 - 0.31C^2 + 0.30D^2$	0.9810	0.9620	4.27	29.803
Compressive strength	$11.35 - 1.85A - 1.26B + 1.32C + 0.95D - 0.65AB - 1.15AC + 0.70AD + 1.93BC - 0.45BD + 0.11CD + 0.057A^2 + 0.54B^2 + 0.96C^2 - 0.97D^2$	0.9815	0.9630	3.62	32.228

Table 5 The results of polynomial variance analysis

Source	Yield stress		Plastic viscosity		Compressive strength	
	F-value	Prob > *F*	*F*-value	Prob > *F*	*F*-value	Prob > *F*
Model	67.29	< 0.0001	49.50	< 0.0001	53.77	< 0.0001
A- fly ash content	0.72	0.4119	84.53	< 0.0001	235.60	< 0.0001
B- water-binder ratio	92.79	< 0.0001	159.41	< 0.0001	102.18	< 0.0001
C- mass concentration	450.97	< 0.0001	164.07	< 0.0001	121.16	< 0.0001
D- superplasticizer dosage	186.94	< 0.0001	152.04	< 0.0001	54.73	< 0.0001
AB	23.84	0.0002	0.59	0.4556	9.69	0.0076
AC	21.52	0.0004	38.44	< 0.0001	30.35	< 0.0001
AD	10.07	0.0068	13.75	0.0023	11.24	0.0047
BC	5.20	0.0388	7.92	0.0138	85.47	< 0.0001
BD	0.54	0.4760	53.14	< 0.0001	7.59	0.0155
CD	2.92	0.1095	1.32	0.2690	0.52	0.4842
A^2	9.62	0.0078	6.21	0.0258	0.05	0.8224
B^2	1.66	0.2183	1.10	0.3110	12.73	0.0031
C^2	44.07	< 0.0001	4.27	0.0577	31.67	< 0.0001
D^2	67.76	< 0.0001	2.95	0.1079	33.58	< 0.0001
Lack of fit	2.86	0.1613	2.87	0.1608	2.73	0.1728

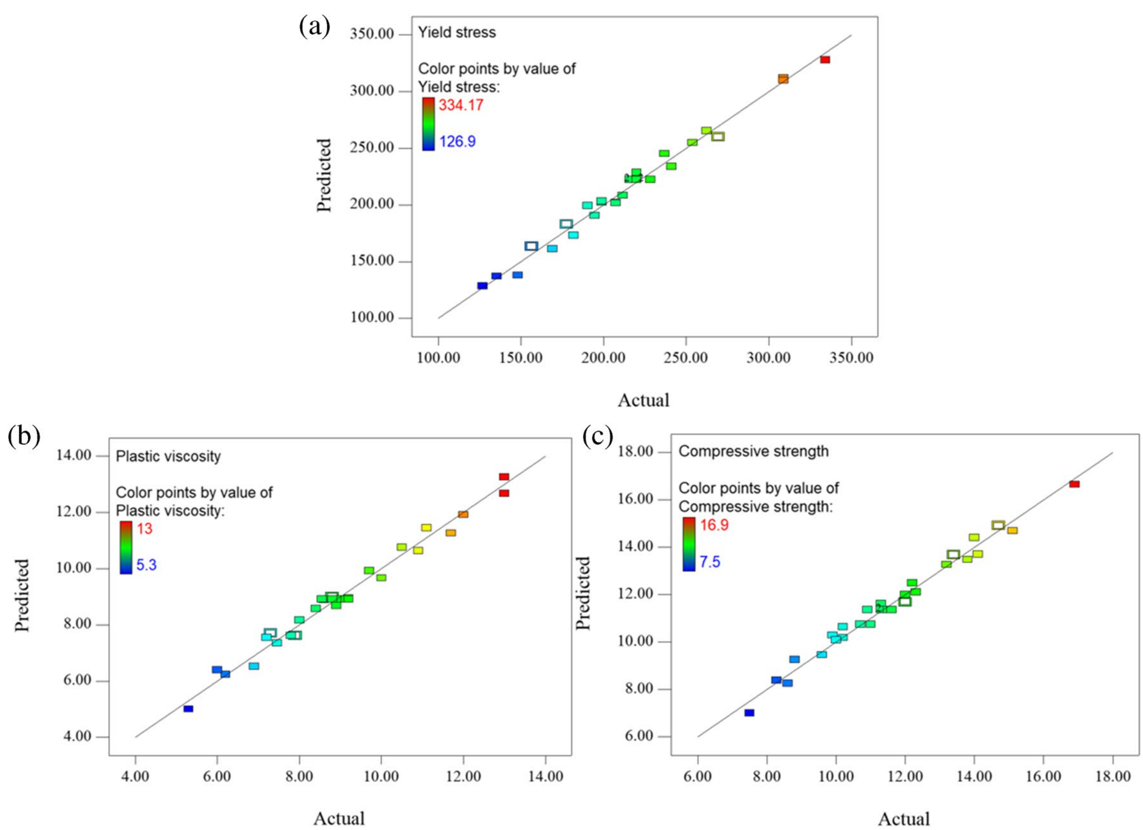

Fig. 6 Predicted vs. actual values for (**a**) yield stress, (**b**) plastic viscosity, and (**c**) compressive strength

Results and discussion

Establishment and analysis of response surface models

The experiment employed an empirical mathematical model in the second-order polynomial form to establish a regression equation for three response values. Subsequently, ANOVA method was conducted to evaluate the multiple correlation coefficient and accuracy of the regression equation, as described in Table 4. The higher the multiple correlation coefficient R^2, the stronger the correlation. A more reliable regression model is obtained when R^2 and R^2_{adj} are high and close to each other. If these values are not high, the presence of other significant influencing factors needs to be considered. C.V. % value less than 10% demonstrates high reliability and precision of the experimental results. Adequate precision is the ratio of effective signal to noise, and if it is greater than 4, the ratio is considered reasonable. Table 5 details the tests performed to determine the significance of various terms in the quadratic equation model, including the constant term, first-order term, second-order term (interaction term), and squared term. A larger F value or a smaller Prob > F value signifies a higher correlation coefficient. For instance, if the Prob > F value is less than 0.05, the model has a high fitting accuracy and is significant, making it appropriate for use in subsequent optimization design (Ahmed 2021). The F values for the lack of fit values for the yield stress, plastic viscosity, and compressive strength were 2.86, 2.87, and 2.73, respectively, which are higher than the Prob > F value, implying that the model's lack of fit was insignificant (Wu et al. 2020a). Tables 4 and 5 show that the yield stress, plastic viscosity, and compressive strength regression models comply with the test principles and exhibit good adaptability.

Validation of the response model

The comparison distribution plot between the predicted values and actual values of the response model is shown in

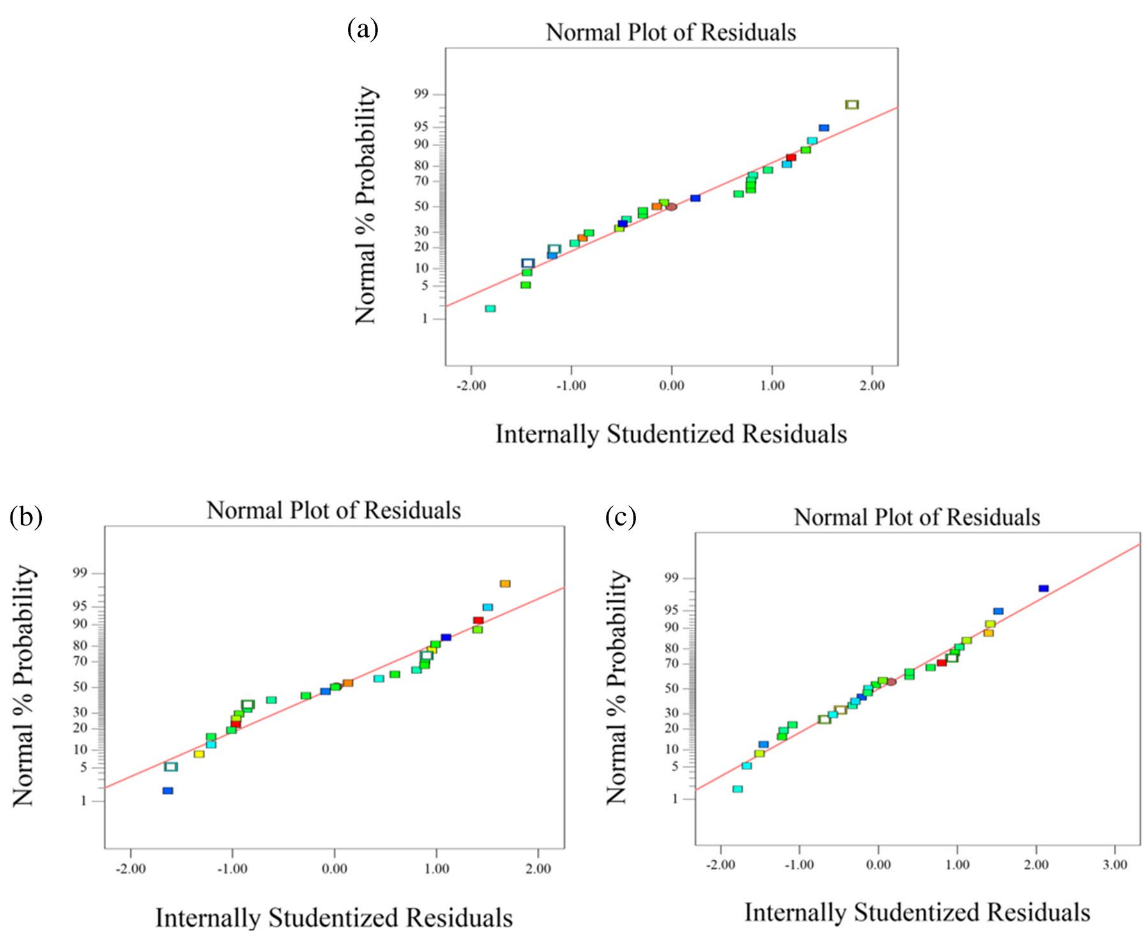

Fig. 7 Normal Plot of Residuals for (**a**) yield stress, (**b**) plastic viscosity, and (**c**) compressive strength

Fig. 6, while the residual distribution plot is shown in Fig. 7 to assess the model's fitting performance. If the model demonstrates good adaptability, the residuals should conform to a normal probability distribution depicted as a straight line, while ensuring that the predicted values closely match the actual values. As shown in Fig. 6 and Fig. 7, the response surface model demonstrated a high degree of agreement with experimental data. Predicted values and actual values were distributed near the straight line, indicating that the regression model can accurately predict the response value (Hu et al. 2022).

Analysis of a single factor

In the analysis of a single factor, the effect of a factor on the response value is studied. The default setting for all factors is intermediate value, serving as the reference point for comparison. Perturbation charts in Fig. 8 illustrate the results of the single-factor analysis for the three factors, with each chart containing four curves. Steep curves indicate a substantial effect on the response value, while relatively flat curves indicate a weak impact. The curve's slope (positive or negative) reflects the trend of the factor's influence on the response value, i.e., whether the response value increases or decreases with an increase of the factor (Yan et al. 2022).

Figure 8 indicates that the critical factor for each of the three response values is different. It can be observed that the yield stress is most sensitive to changes in mass concentration, but insensitive to variations in fly ash content, according to Fig. 8(a). From Fig. 8(b), it can be observed that the plastic viscosity is mainly influenced by the mass concentration, which is also sensitive to changes in water-cement ratio and superplasticizer dosage. The impact of fly ash content and mass concentration is most significant for compressive strength, as shown in Fig. 8(c). During the optimization process, it is not possible to adjust every parameter to its optimal level due to real-world limitations. Therefore, prioritizing the dominant factors and determining a final optimization plan within a feasible range are necessary.

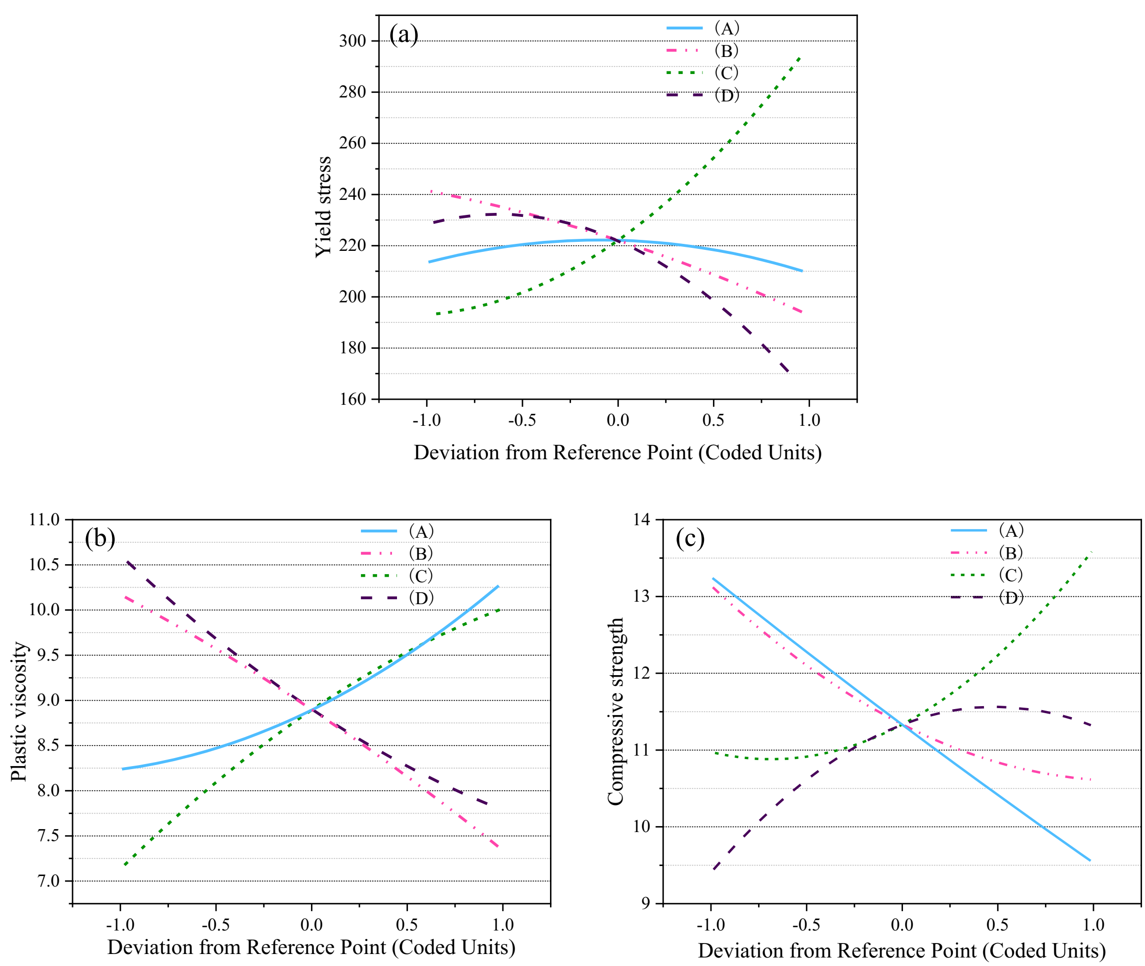

Fig. 8 Perturbation plot for (**a**) yield stress, (**b**) plastic viscosity, and (**c**) compressive strength

Analysis of interaction effects among factors

The Design-Export software generated two-dimensional contour maps and three-dimensional response surface plots that depict the interaction effects between independent variables and their corresponding response values based on the quadratic model. The graphs allow evaluation of the interaction effects between any two factors by holding the remaining two factors constant. Red and blue colors represent the highest and lowest response values, respectively.

The influence of interaction effects on the yielding stress

The yielding stress of slurries is primarily caused by the adhesion and frictional forces between the surface of the material particles, which is the maximum stress that impedes the plastic deformation of the slurry (Zheng et al. 2022). Table 5 presents the order of significance of the independent variables affecting the yielding stress as follows: mass concentration (C) > superplasticizer dosage (D) > water-cement ratio (B) > fly ash content (A). Figure 9(a) and (a') shows the interaction effect of fly ash content and water-cement ratio on the yielding stress. It can be observed that the yielding stress decreases with an increase in the water-cement ratio and increases slowly with an increase in fly ash content. This is because fly ash replaces cement particles, reducing their density, and thus reducing the formation of flocculent hydration products between cement particles. Meanwhile, the glass microspheres in fly ash act as a lubricant, reducing the yielding stress. The results plotted in Fig. 9(b) and (b') indicate that mass concentration has a more notable effect on the yielding stress than other factors. Initially, stress increases gradually with increasing mass concentration but sharply rises beyond a mass concentration of 80%. A high water-cement ratio produces more free water, which fly ash, with its larger specific surface area, absorbs together with more free water and superplasticizer, resulting in an increased slurry density and more tightly packed

Fig. 9 Response surface plots and contour maps of interaction between different variables to yield stress

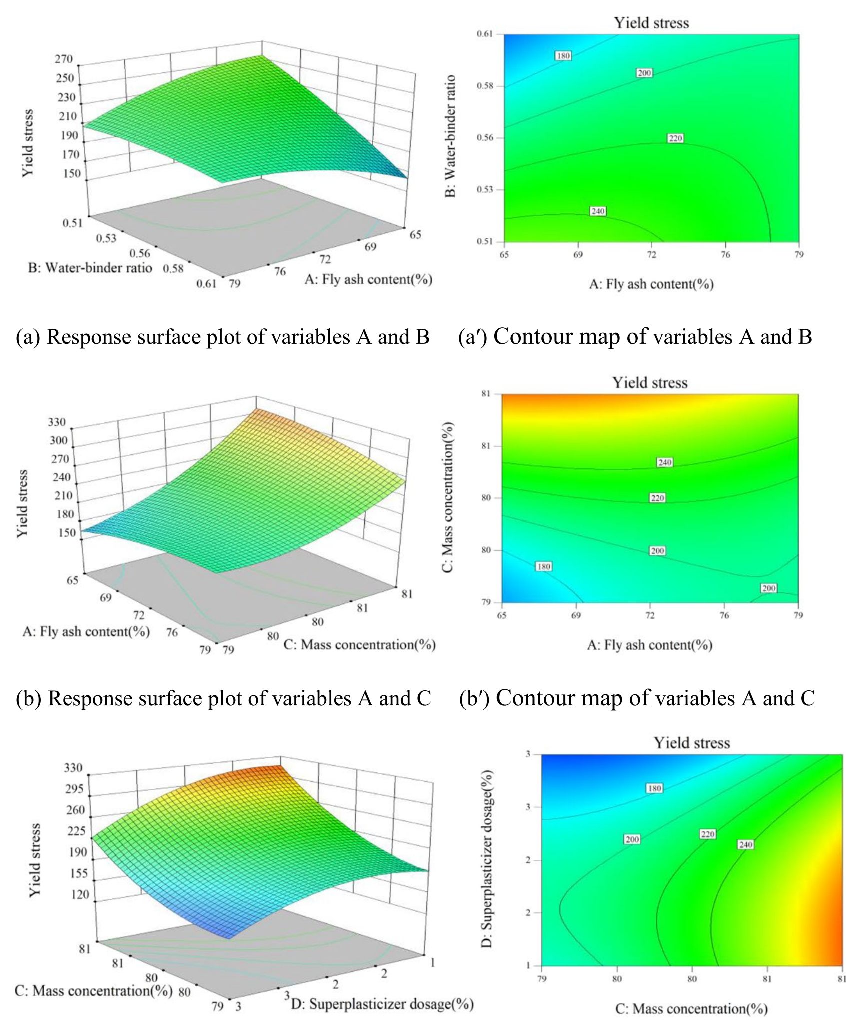

(a) Response surface plot of variables A and B (a′) Contour map of variables A and B

(b) Response surface plot of variables A and C (b′) Contour map of variables A and C

(c) Response surface plot of variables C and D (c′) Contour map of variables C and D particles forming a floc-like structure due to the van der Waals force attraction with cement/ultrafine gangue/fly ash, creating a stronger cohesive force. Figure 9(b') illustrates that the maximal yielding stress occurs when the fly ash content represents 66%, and the mass concentration equals 81%, located in the top-left corner of the contour plot. Figure 9(c) and (c') reveals the interaction effect of mass concentration and superplasticizer dosage on the yielding stress. When the mass concentration decreases and the superplasticizer dosage increases, the yielding stress decreases. With an increase in the superplasticizer dosage, the yielding stress first decreases slowly and then rapidly. The decrease in mass concentration will result in a reduction in the amount of binding materials and aggregates in the slurry, and consequently an increase in the spacing between cement particles. The hydrophobic bases of the superplasticizer molecule can adsorb on the surface of cement and fly ash particles, making them carry the same charge, thereby generating repulsion and dispersing the particles, intensifying the particle Brownian diffusion movement, releasing more free water. This effect reduces the generation of a floc-like structure, leading to a decrease in yielding stress (Liu et al. 2022).

The influence of interaction on plastic viscosity

Plastic viscosity is the viscous force that prevents the flow of each laminar flow layer in the slurry in the opposite direction. It depends on the degree of destruction of the interlaced reticulated structure formed by interconnected cement and fly ash particles through van der Waals forces and electrostatic interactions (Wu et al. 2020b). Table 5 shows the significant order of each independent variable affecting on plastic viscosity: mass concentration (C) > water-cement ratio (B) > fly ash content (A) > superplasticizer dosage (D). Figure 10(a) and (a') shows the interactive effect of fly ash content and water-cement ratio on plastic viscosity. As the increase of fly ash content and mass concentration, the plastic viscosity increases, but as the water-cement ratio increases, the plastic viscosity decreases. This is because fly ash particles have a smaller particle size, which can fill

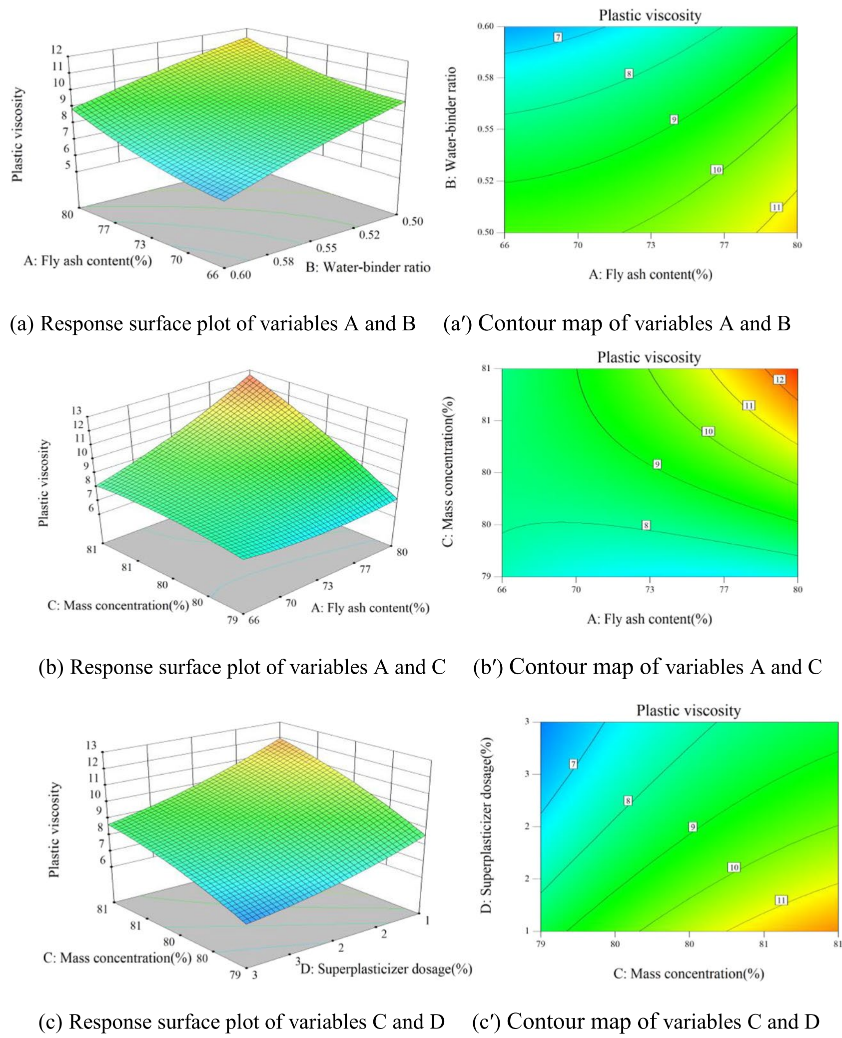

(a) Response surface plot of variables A and B (a′) Contour map of variables A and B

(b) Response surface plot of variables A and C (b′) Contour map of variables A and C

(c) Response surface plot of variables C and D (c′) Contour map of variables C and D

Fig. 10 Response surface plots and contour maps of interaction between different variables to plastic viscosity some of the gaps between the cement particles, increasing the particle density (Bentz et al. 2012; Gullu et al. 2019). As the water-binder ratio increases and the mass concentration remains constant, the amount of aggregate increases. This means that more mortar is needed to cover the aggregate. The increased amount of aggregate leads to more collisions between them. Additionally, larger aggregates can impact the formation of particle clusters and reticulated structures in the slurry, resulting in a reduction in the plastic viscosity. At the same time, because the specific surface area of fly ash is greater than that of cement, it can absorb more water, leading to a decrease in the thickness of the water film on the surface of the particles, which increases the plastic viscosity. The results depicted in Fig. 10(b) and (b') demonstrate a significant relationship between mass concentration and plastic viscosity when the fly ash content is 80%. The data presented in Fig. 10(c) and (c') indicate that increasing the superplasticizer dosage results in lower plastic viscosity and decreased reticulated structure of cement slurry, resulting in easier flow of the slurry.

The influence of interaction on compressive strength

The impact of interactions on the compressive strength can be seen through the response surface plots and contour maps presented in Fig. 11. Table 5 shows the significant order of each independent variable affecting on compressive strength: fly ash content (A) > mass concentration (C) > water-cement ratio (B) > superplasticizer dosage (D). Figure 11(a) and (a') indicates that when the mass concentration and superplasticizer dosage remain constant, the compressive strength decreases with the increase of fly ash content and water-cement ratio. This is because the increase in fly ash content reduces the amount of cement, leading to a decrease in the number of ettringite crystals generated during the 28-day aging period and resulting in a decrease in strength. In addition, the increase in water-cement ratio reduces the proportion of binding material, leading to a lower compressive strength. Figure 11(b) and (b') demonstrates that when the water-cement ratio and superplasticizer dosage remain constant, the compressive

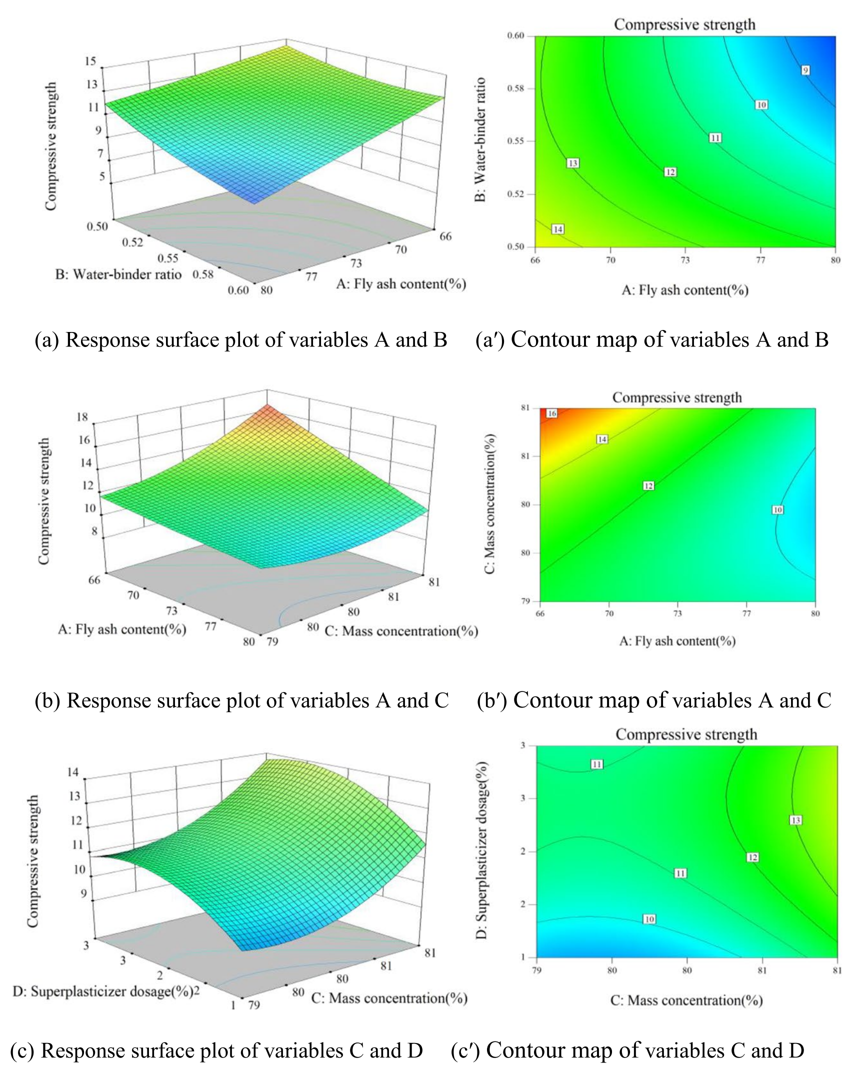

Fig. 11 Response surface plots and contour maps of interaction between different variables to compressive strength

strength first increases slowly, and then rapidly increases with the increase of mass concentration. This is because the increase in mass concentration increases the amount of binding material and aggregate, which reduces the proportion of free water and decreases the number of cracks and void spaces produced by free water during the hardening process, thereby improving the compactness of the specimen (Zhao et al. 2022). Figure 11(c) and (c') shows that the compressive strength first increases slowly with the increase of superplasticizer dosage, and gradually stabilizes when the content reaches 2%. This is because polycarboxylate superplasticizer has a strong dispersing effect, which can increase the filling density of binding material and increase the thickness of the water film, thus promoting the hydration of cement. However, when the content of superplasticizer dosage exceeds 2%, the degree of dispersion increases to its maximum, and the improvement in filling density decreases, resulting in a gradual increase in strength (Zhang et al. 2023).

Multi-objective optimization of filling material mix proportions

To ensure good pumpability of the slurry during pipeline transport and to guarantee the filling material meets the mining filling requirements, this paper adopts a model based on RSM to optimize the proportion of CGBM. The goals selected for the optimization were the minimum yielding stress and plastic viscosity, and the maximum value of the compressive strength. A multi-objective optimization algorithm was applied to search for the optimal point that maximizes the expected function within a numerical optimization range from 0 to 1 in Eq. (7).

$$D = (d_1 d_2 ... d_n)^{1/n} = \left(\prod_{i=1}^{n} d_i\right)^{1/n} \tag{9}$$

where D is the satisfaction of the expected function; n is the number of response values; d is the satisfaction of a single response value.

By adjusting the weight of each response value (Tippawan et al. 2022), the optimization objective can be changed. In this paper, the optimization objective is to make yield stress a low response, and plastic viscosity and compressive strength high responses. To achieve optimization of the proportion of CGBM, each response value is assigned a corresponding importance. Each response value is weighted to obtain the final optimized proportion, as shown in Table 6. Under the optimal ratio, the fly ash content is 80%, the mass concentration is 79%, the water-cement ratio is 54%, and the superplasticizer dosage is 3%. At this point, the response values are the following: yield stress of 162.1 Pa, plastic viscosity of 7.3 Pa·s, and compressive strength of 12.0 MPa.

Table 6 Optimum conditions, observed and predicted value of response at optimized conditions

Independent variables	Goal	Importance	Optimum conditions
A- fly ash content	Maximize	+ +	80
B- water-binder ratio	Maximize	+	54
C- mass concentration	Minimize	+	79
D- superplasticizer dosage	Maximize	+ + +	3
Responses			Predicted values
Yield stress	Minimize	+ +	162.1
Plastic viscosity	Minimize	+ + +	7.3
Compressive strength	Maximize	+ +	12.0

Conclusion

In this study, response surface methodology was employed to investigate the effects of different fly ash content, water-to-cement ratio, mass concentration, and dosage of high-efficiency water reducer on the rheological properties of CGBM. Additionally, the optimization of the mixture proportion was conducted.

(1) A second-order polynomial model based on response surface methodology was established to examine the influence of fly ash content, water-to-cement ratio, mass concentration, and the amount of high-efficiency water reducer on the rheological property of CGBM. The model demonstrates a high degree of predictive accuracy.
(2) The rheological and mechanical properties of CGBM are influenced by the interaction among multiple factors. An increase in mass concentration leads to a significant rise in the yield stress and plastic viscosity of CGBM. The interaction between fly ash content and water-to-binder ratio significantly affects the yield stress. Among all factors, the fly ash content has the most significant influence on the compressive strength. Additionally, a dosage of superplasticizer between 2 and 3% improves fluidity and simultaneously enhances the hardened compressive strength.
(3) Based on the results of the multi-objective optimization, the optimal ratio of CGBM is a fly ash content of 80%, water-binder ratio of 54%, mass concentration of 79%, and superplasticizer dosage of 3%. The optimization results are significant in guiding the selection of the optimal mix proportion in preparing CGBM.

It is necessary to further investigate the pressure loss of different CGBM slurries in pipeline transportation during the backfilling process. Additionally, the impact of environmental factors on CGBM should be taken into consideration.

Author contribution Xiaoxuan Wang: experiment, data collection and drafting. Yuxia Guo: funding acquisition, methodology, and supervising all stages of manuscript preparation. Guorui Feng: investigation, financing and supervision. Xiaoli Ye, Weiyang Hu, and Jiahui Ma: supervision, review, editing and conceptualization. All authors have read, revised, approved, and agreed to the contents of the final version of this review.

Funding This study was sponsored by the National Natural Science Foundation of China (Grant No. 51974192), the Distinguished Youth Funds of National Natural Science Foundation of China (Grant No. 51925402), and Shanxi-Zheda Institute of Advanced Materials and Chemical Engineering Project (2022SX-TD007).

Data availability The datasets used and/or analyzed during the current study are available from the corresponding author on reasonable request.

Declarations

Competing interests The authors declare no competing interests.

References

Ahmed J (2021) Effect of pressure, concentration and temperature on the oscillatory rheology of guar gum dispersions: response surface methodology approach. Food Hydrocoll 113:106554. https://doi.org/10.1016/j.foodhyd.2020.106554

Allaix DL, Carbone VI (2011) An improvement of the response surface method. Struct Saf 33:165–172. https://doi.org/10.1016/j.strusafe.2011.02.001

Asr ET, Kakaie R, Ataei M, Mohammadi MRT (2019) A review of studies on sustainable development in mining life cycle. J Clean Prod 229:213–231. https://doi.org/10.1016/j.jclepro.2019.05.029

Bentz DP, Ferraris CF, Galler MA, Hansen AS, Guynn JM (2012) Influence of particle size distributions on yield stress and viscosity of cement–fly ash pastes. Cem Concr Res 42:404–409. https://doi.org/10.1016/j.cemconres.2011.11.006

Chugh YP, Behum PT (2014) Coal waste management practices in the USA: an overview. Int J Coal Sci Technol 1:163–176. https://doi.org/10.1007/s40789-014-0023-4

Deng X, Zhang J, Klein B, Zhou N, Dewit B (2017) Experimental characterization of the influence of solid components on the rheological and mechanical properties of cemented paste backfill. Int J Miner Process 168:116–125. https://doi.org/10.1016/j.minpro.2017.09.019

Dong HZ, Feng GR, Guo YX, Qi TY, Kang LX, Guo XY, Han YL (2013) Pipe transportation characteristics of filling slurry in Xinyang mine. J Min Saf Eng 30(06):880–885 (**CNKI:SUN:KSYL.0.2013-06-015**)

Faravelli L (1989) Response-surface approach for reliability analysis. J Eng Mech 115:2763–2781. https://doi.org/10.1061/(ASCE)0733-9399(1989)115:12(2763)

Fei J (1997) Study of nondeposit velocity in slurry pipeline. J China Coal Soc 22:532–536. https://doi.org/10.13225/j.cnki.jccs.1997105.018. (In Chinese)

Feng G, Jia X, Guo Y, Qi T, Li D, Li Z, Feng J, Liu G, Song K, Kang L (2015) Influence of the wasted concrete coarse aggregate on the performance of cemented paste backfill. J China Coal Soc 40:1320–1325. https://doi.org/10.13225/j.cnki.jccs.2015.305. (In Chinese)

Feng G, Du X, Guo Y, Qi T, Wang Z, Li Q, Li H, Kang L (2019) Basic theory of constructional backfill mining and the underground space utilization concept. J China Coal Soc 44:74–84. https://doi.org/10.13225/j.cnki.jccs.2018.1598. (In Chinese)

Feng G, Wang Z, Qi T, Du X, Guo J, Wang H, Shi X, Wen X (2022) Effect of velocity on flow properties and electrical resistivity of cemented coal gangue-fly ash backfill (CGFB) slurry in the pipeline. Powder Technol 396:191–209. https://doi.org/10.1016/j.powtec.2021.10.050

Feys D, Wallevik JE, Yahia A, Khayat KH, Wallevik OH (2013) Extension of the Reiner-Riwlin equation to determine modified Bingham parameters measured in coaxial cylinders rheometers. Mater Struct 46:289–311. https://doi.org/10.1617/s11527-012-9902-6

GB/T 50081–2002 (2002) Standard for test method of mechanical properties on ordinary concrete. China Architecture and Building Press, Beijing, China

Gullu H, Cevik A, Al-Ezzi KMA, Gulsan ME (2019) On the rheology of using geopolymer for grouting: a comparative study with cement-based grout included fly ash and cold bonded fly ash. Constr Build Mater 196:594–610. https://doi.org/10.1016/j.conbuildmat.2018.11.140

Guo X (2013) The study of influencing factors of paste filling performance, Dissertation, Taiyuan University of Technology, Taiyuan, China (In Chinese)

Hu Y, Li K, Han B, Li H, Zhao J (2022) Strength development and optimization analysis of mixed aggregate backfill based on RSM-DF. J Cent South Univ (Science and Technology) 53(2):620–630. https://doi.org/10.11817/j.issn.1672-7207.2022.02.025. (In Chinese)

Hua X, Chang G, Liu X, Yang K, Chen D, Li C, Wang E (2022) Strength evolution law and acoustic-emission characteristics of multi-source coal-based filling body of solid wastes. Chin J Rock Mech Eng 41:1536–1551. https://doi.org/10.13722/j.cnki.jrme.2021.1264. (In Chinese)

Jiang H, Fall M, Yilmaz E, Li Y, Yang L (2020) Effect of mineral admixtures on flow properties of fresh cemented paste backfill: assessment of time dependency and thixotropy. Powder Technol 372:258–266. https://doi.org/10.1016/j.powtec.2020.06.009

Li P, Hou Y, Cai M (2019a) Factors influencing the pumpability of unclassified tailings slurry and its interval division. Int J Miner Metall Mater 26:417–429. https://doi.org/10.1007/s12613-019-1750-8

Li Q, Feng G, Guo Y, Qi T, Du X, Wang Z, Li H (2019b) The dosage of superplasticizer in cemented coal waste backfill material based on response surface methodology. Adv Mater Sci Eng 2019:5328523. https://doi.org/10.1155/2019/5328523

Liu L, Ji Y, Li L, Zhang J (2022) Influences of CO2 absorption under ultrasonic vibration and water-reducer addition on the rheological properties of cement paste. Appl Sci-Basel 12:3739. https://doi.org/10.3390/app12083739

Ma Z, Fan J, Sun K, Zhao G, Pan Y (2011) Study on stope stability during repeated mining with fully-mechanized solid filling technology in residual coal pillar area. J Min Saf Eng 28(4):499–504+510. https://doi.org/10.3969/j.issn.1673-3363.2011.04.001. (In Chinese)

Qi T, Gao X, Feng G, Bai J, Wang Z, Chen Q, Wang H, Du X (2022) Effect of biomass power plant ash on fresh properties of cemented coal gangue backfill. Constr Build Mater 340 https://doi.org/10.1016/j.conbuildmat.2022.127853

Qian M, Miao X, Xu J (2007) Green mining of coal resources harm on izing with environment. J China Coal Soc 32(1):1–7. https://doi.org/10.13225/j.cnki.jccs.2007.01.001. (In Chinese)

Reng A, Feng G, Guo Y, Qi T, Guo J, Zhang M, Kang L, Han Y, Zhang P (2014) Influence on performance of coal mine filling paste with fly ash. J China Coal Soc 39:2374–2380. https://doi.org/10.13225/j.cnki.jccs.2013.1747. (In Chinese)

Sun Q, Tian S, Sun Q, Li B, Cai C, Xia Y, Wei X, Mu Q (2019) Preparation and microstructure of fly ash geopolymer paste backfill material. J Clean Prod 225:376–390. https://doi.org/10.1016/j.jclepro.2019.03.310

Tippawan P, Jienkulsawad P, Limleamthong P, Arpornwichanop A (2022) Composting time minimization of mature vermicompost using desirability and response surface methodology approach. Comput Chem Eng 167:108037. https://doi.org/10.1016/j.compchemeng.2022.108037

Wang H, Zhang G, Wu A, Yang P, Peng N, Yang X, Zhou F (2014) Study on rheological properties of paste with different corase aggregate. Min Res Dev 34:59–62. https://doi.org/10.13827/j.cnki.kyyk.2014.07.015. (In Chinese)

Wang H, Wang X, Kou Y, Wu Z, Peng Q (2021) Loop test study on the high-concentration cemented filling of full tailings. Chin J Eng 43(2):215–222. https://doi.org/10.13374/j.issn2095-9389.2020.01.09.002. (In Chinese)

Wu D, Zhang Y, Liu Y (2016) Mechanical performance and ultrasonic properties of cemented gangue backfill with admixture of fly ash. Ultrasonics 64:89–96. https://doi.org/10.1016/j.ultras.2015.08.004

Wu A, Ruan Z, Bürger R, Yin S, Wang J, Wang Y (2020a) Optimization of flocculation and settling parameters of tailings slurry by response surface methodology. Miner Eng 156:106488. https://doi.org/10.1016/j.mineng.2020.106488

Wu B, An X, Shi C, Wei Z, Yuan Q (2020b) Effect of rheological properties on stability and appearance of cast concrete. Mater Rep 34(04):4043–4048. https://doi.org/10.11896/cldb.19010196. (In Chinese)

Xu W, Tian X, Hou Y, Wei S, Yue R, Fan P, Zhu S, Yin T (2016) Experimental study on the pore and strength properties of cemented unclassified during the consolidation process. J China Univ Min Technol 45(2):272–279. https://doi.org/10.13247/j.cnki.jcumt.000481. (In Chinese)

Yan W, Meng X, Cui X, Liu Y, Chen Q, Jin L (2022) Evaporative cooling performance prediction and multi-objective optimization for hollow fiber membrane module using response surface methodology. Appl Energy 325:119855. https://doi.org/10.1016/j.apenergy.2022.119855

Yang T, Qiao D, Wang J, Zhang X, Chen Y (2021) Numerical simulation and new model of pipeline transportation resistance of waste rock-aeolian sand high concentration slurry. Chin J Nonferrous Met 31(1):234–244. https://doi.org/10.11817/j.ysxb.1004.0609.2021-36517. (In Chinese)

Ye X, Guo Y, Feng G, Wang X, Hu W, Ma J (2023) Rheological properties of cemented gangue backfill material based on fractal characteristics of waste coal gangue. Environ Sci Pollut Res Int. https://doi.org/10.1007/s11356-023-25452-4

Yilmaz E, Belem T, Benzaazoua M (2014) Effects of curing and stress conditions on hydromechanical, geotechnical and geochemical properties of cemented paste backfill. Eng Geol 168:23–37. https://doi.org/10.1016/j.enggeo.2013.10.024

Yin S, Wu A, Hu K, Wang Y, Zhang Y (2012) The effect of solid components on the rheological and mechanical properties of cemented paste backfill. Miner Eng 35:61–66. https://doi.org/10.1016/j.mineng.2012.04.008

Zhang Y, Ma Z, Zhi X, Chen X, Zhou J, Wei L, Liu Z (2023) Damage characteristics and constitutive model of phosphogypsum/fly ash/ slag recycled aggregate concrete under uniaxial compression. Cem Concr Compos 138:104980. https://doi.org/10.1016/j.cemconcomp.2023.104980

Zhao Y, Guo Y, Feng G, Li C, Xie W, Zhang C (2022) Study on strength and deformation characteristics of cemented gangue backfill body under the coupling action of load and salt erosion. Constr Build Mater 342:128003. https://doi.org/10.1016/j.conbuildmat.2022.128003

Zheng B, Zhou H, He R (2006) Experimental research on coal gangue paste filling material. J Min Saf Eng 23:460–463. https://doi.org/10.3969/j.issn.1673-3363.2006.04.019(InChinese)

Zheng X, Han F, Liu J, Liu J, Sha J, Lin W (2022) Rheological properties and stability of ultra-high performance concrete containing coarse aggregate. J Chin Ceram Soc 50(11):2844–2854. https://doi.org/10.14062/j.issn.0454-5648.20220254. (In Chinese)

Zhu L, Jin Z, Zhao Y, Duan Y (2021) Rheological properties of cemented coal gangue backfill based on response surface methodology. Constr Build Mater 306:124836. https://doi.org/10.1016/j.conbuildmat.2021.124836